Radiologic Imaging of the Ankle

Alexander B. Peterson and Eric W. Tan

When evaluating the ankle, the proper use of diagnostic imaging is critical for accurate diagnosis and guiding the appropriate treatment. This chapter will discuss imaging techniques that are commonly used to assess the ankle. This encompasses traditional modalities, such as radiography, magnetic resonance imaging (MRI), and computed tomography (CT), as well as more specialized techniques including weight bearing CT (WBCT) and single photon emission computed tomography (SPECT) scans.

1 Radiography

Radiographs, colloquially known as X-rays, are the most utilized form of imaging in the foot and ankle. Image acquisition is rapid, cost is relatively inexpensive, and the required equipment can be readily installed in the office setting. In the modern era, digital radiography has replaced conventional film-based radiographs. At its core, radiographs are produced by passing ionizing radiation, such as X-rays, through a patient. The penetration of the radiation is variable based on the density of the tissue, with bone and metallic implants generally being the densest. The penetrating radiation effectively produces a shadow of the anatomy, which is captured on the detector. Detectors were traditionally photographic film but are now commonly digital. The digital detector then produces the radiographic image for diagnostic interpretation [1, 2].

A thorough history and physical examination is critical for guiding the decision to obtain radiographic imaging. Beyond standard radiographs of the ankle, the history and exam may guide the practitioner to order special views, stress views, or images of adjacent anatomy, such as the foot, tibia and fibula, or full-length films of the limb. In general, radiographs provide a good initial evaluation of the ankle joint and can direct the need for more advanced imaging studies, as needed.

Due to a concern that radiographs were being overutilized to evaluate ankle injuries, the Ottawa rules were developed to guide practitioners on the proper use of radiographic examination in the setting of an acute ankle injury [3]. As most ankle injuries are sprains that do not involve fractures of the bones, unnecessary X-rays may be avoided by following restrictions laid forth by the Ottawa guidelines. These rules are defined as bony tenderness at the malleoli or the inability to bear weight; if any of these are present, radiographic assessment is warranted. Sensitivity of this decision-making tool has been shown to be 100% for fractures, with moderate specificity. When implemented in clinical practice, the rate of ankle radiographs is reduced by up to 40% [4–6].

A. B. Peterson · E. W. Tan (✉)
Department of Orthopaedic Surgery, Keck School of Medicine of USC, Los Angeles, CA, USA
e-mail: Alexander.Peterson@med.usc.edu; Eric.Tan@med.usc.edu

D. Herscovici Jr. et al. (eds.), *Evaluation and Surgical Management of the Ankle*,
https://doi.org/10.1007/978-3-031-33537-2_3

Ottawa ankle rules are effective for ruling out unstable ankle fractures in the acute setting, arguably making them appropriate in the emergency department, but radiographs are useful for more than detecting fractures. As such, the authors have a low threshold to obtain ankle radiographs, which can provide information about potential arthritis, focal articular lesions, anatomic alignment, tumors, infection, and certain soft tissue conditions, among others. It is also important to point out that patients may present with ankle pain in the absence of trauma.

If imaging is warranted, standard views of the ankle are obtained. These include anteroposterior (AP), lateral, and internal oblique (mortise) views (Fig. 1). Whenever possible, standing (i.e., weight-bearing) radiographs are obtained in lieu of non-weight-bearing films. Weight-bearing radiographs provide important information about the overall structural alignment of the ankle as it exists in daily life. In most cases, it is when the patient is using and loading the ankle that they experience pain or discomfort. Therefore, the weight-bearing images create the physiologic stresses on the ankle joint and surrounding ligaments that illustrate key findings like joint space narrowing, bony impingement, and joint subluxation that would go unappreciated in a non-weight-bearing radiograph. Non-weight-bearing films should only be obtained when the patient is unable to stand on the limb, either due to pain or other physical restriction.

The *AP view*, with the knee and the axis of the first ray of the foot pointing forward, allows evaluation of the tibiotalar joint, distal tibia and fibula, peripheral borders of the tarsals, talar dome, and the syndesmosis (Fig. 2) [7, 8]. The lateral gutter is poorly visualized due to overlap between the fibula and the lateral aspect of the talus.

The *mortise view*, or internal oblique, is obtained with the leg internally rotated 15–20° relative to the AP position. There should be no overlap of the malleoli with the talus [9]. It provides additional information about the ankle mortise and syndesmotic alignment, talar dome integrity, different views of the malleoli, and allows for inspection of the lateral talar process. The mortise view produces the optimal assessment of tibiotalar and talofibular congruity.

The *lateral view* is obtained with the medial border of the foot against the cassette and the beam perpendicular. A true lateral has perfect overlap of the medial and lateral talar dome, and no overlap between the tibial plafond and the talar dome. The fibula will be superimposed on the tibia. It allows for assessment of the ankle for effusion, hindfoot integrity and talocalcaneal relationship, tibiofibular integrity and syndesmosis, and tibiotalar congruity. In the case of fracture, particular attention should be paid to the posterior malleolus. The fifth metatarsal base, often fractured from inversion injuries, may also be well-visualized on a lateral radiograph.

At some institutions, an *external oblique radiograph* is included in the standard trauma series. To obtain this view, the leg is rotated externally 45°, relative to a true AP [7]. This allows for improved assessment of the posterior colliculus of the medial malleolus, which can otherwise be difficult to visualize [10].

If an isolated medial or posterior malleolar ankle fracture or isolated medial clear space widening is identified, it is critical that the practitioner examines the entire lower leg and obtains films of the complete tibia and fibula to rule out a Maisonneuve injury-pattern with a more proximal fibula fracture (Fig. 3).

When obtaining a non-weight-bearing image, the ankle should be dorsiflexed to neutral, with some pronation through the foot to create a more physiologic view [7]. Due to the normal anatomy of the talus, it is broader anteriorly than posteriorly, so if the talus is plantarflexed during the AP or mortise radiographs, the medial clear space measurements may be distorted. Stress views of the ankle are also important diagnostic tools in cases when the patient is unable to bear weight.

1.1 Radiographic Evaluation

It is important to understand the measurements commonly applied to the standard ankle series, particularly in the setting of trauma, with most establishing the stability status of the ankle

Fig. 1 Standard radiographic weight-bearing views of the ankle. (**a**) Anteroposterior. (**b**) Mortise. (**c**) Lateral

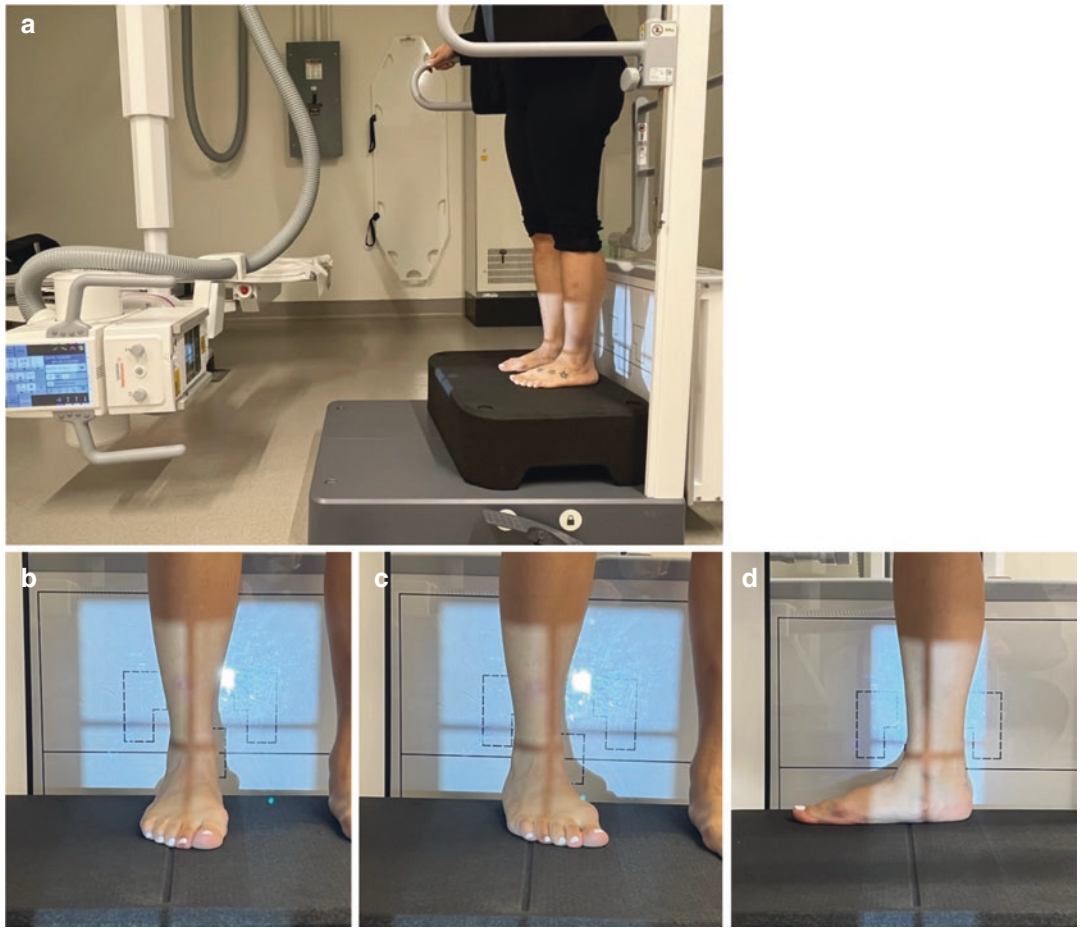

Fig. 2 Techniques for the acquisition of standard weight-bearing radiographs of the ankle. (**a**) The patient stands on an elevated platform between the beam and the cassette. The beam is angled parallel to the floor. (**b**) Anteroposterior view: The first ray and patella are pointed forward, parallel to the beam. (**c**) Mortise view: The leg is internally rotated 15–20°. (**d**) Lateral view: the first ray is oriented perpendicular to the beam

following fracture or ligamentous disruption. The *medial clear space* gives information about the integrity of the deltoid ligament. Measured on a weight-bearing or stress mortise view, it is defined as the distance between the medial border of the talus and the lateral border of the medial malleolus (Fig. 4) [9, 11]. Specifically, the measurement should be made 5 mm distal to the dome of the talus [12]. Values >5 mm or >1 mm greater than the tibiotalar distance (between the tibial plafond and talar dome) have been proposed at cutoffs for clinically significant deltoid injury [13, 14]. Practically, this could lead a surgeon to fixation of the fibula in an unstable isolated lateral malleolus fracture. The *tibiofibular clear space* and the *tibiofibular overlap* assess the ligaments, integrity and alignment of the syndesmosis and can also be measured on weight-bearing or stress views. The *tibiofibular clear space* is measured from the medial border of the fibula to the incisura fibularis (tibial concavity at the distal tibiofibular articulation) [15]. It is measured 1 cm proximal to the tibial plafond [16]. Widening represents potential disruption of the ankle syndesmosis, either through fracture or frank ligamentous injury (such as a "high ankle sprain"). Traditionally, normal values were considered normal if they were less than 6 mm on AP and mortise views. *Tibiofibular overlap* measures the radiographic overlay of the fibula and the anterolateral fibula on AP and mortise views. Again, it is measured 1 cm proximal to the tibial

Fig. 3 Maisonneuve injury pattern. (**a**) Isolated medial clear space widening is seen on the initial radiographs. (**b**) Tibia fibula films demonstrate a fracture of the proximal fibula, consistent with a Maisonneuve injury with syndesmotic disruption

plafond. Normal values are traditionally >6 mm on the AP view and >1 mm on the mortise view. Though helpful for guiding evaluation, these values for tibiofibular clear space and overlap have been challenged, as significant variation has been found in normal controls [15]. The *anterior to posterior fibular gap* is specific to rotational ankle fractures and is measured on the lateral view. The orthogonal distance between the proximal and distal fibula fragments is measured, immediately anterior to the disruption in the posterior cortex [14]. Values greater than 1 mm on initial injury radiographs are associated with medial tibiotalar instability.

Fig. 4 Common radiographic measurements of the ankle. *Medial clear space* (cyan arrow) is measured 5 mm below the level of the talar dome, between the medial aspect of the talus and the lateral aspect of the medial malleolus. *Tibiofibular clear space* (red arrow) is measured 1 cm proximal to tibial plafond, between the medial border of the fibula and the medial shadow of the incisura fibularis (green line). *Tibiofibular overlap* (yellow arrow) is measured 1 cm proximal to the tibial plafond, between the lateral border of the tibia (magenta line) and the medial border of the fibula

1.2 Stress Radiographs

Plain radiographs may not adequately identify the presence of any associated soft tissue injuries. To evaluate these injuries, stress radiographs have been described. Stress radiographs assess ligamentous instability and may be considered for acute or chronic ankle injuries. To evaluate distal syndesmotic or medial ankle deltoid ligament tears, especially in setting of a fibula fracture, the use of *gravity stress* or *manual external rotation stress* radiographs have been described [11, 17]. The purpose of these two stress radiographs is to guide the practitioner in determining both the optimal treatment (operative versus nonoperative care) and the recommended weight-bearing status. When positive, the images will demonstrate relative widening of the medial clear space, indicative of a deltoid injury, and/or widening of the tibiofibular joint, indicative of a syndesmotic injury. It is not uncommon for a distal fibula fracture to have a stable appearance on a non-weight-bearing mortise view, only to have significant subluxation on a stress exam. Gravity stress radiographs are performed with the patient in the lateral decubitus position, injured side down. The limb's rotation and the beam are adjusted to obtain a mortise view of the ankle (Fig. 5). It is imperative that the medial malleolus is closer to the ceiling and the lateral malleolus closer to the ground. This allows the foot and talus, under their own weight (gravity), to "fall down" away from the medial malleolus. The *manual external rotation stress* is obtained by stabilizing the tibia with one hand, while applying a steady external rotational

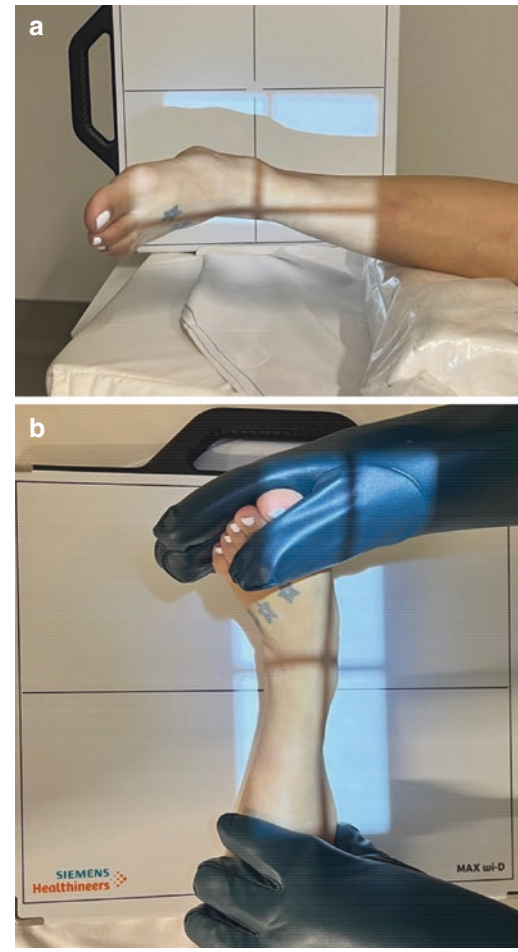

Fig. 5 Ankle stress tests are used to diagnose joint instability. (**a**) Gravity stress view: The affected ankle is suspended, with the medial side toward the ceiling. A mortise view is obtained. (**b**) Manual external rotation stress: Utilizing lead gloves to avoid unnecessary radiation exposure, the provider stabilizes the leg while applying an external rotation force through the foot

force through the foot, preferably in neutral to slight dorsiflexion during a mortise radiograph [18, 19]. It is best practice for the practitioner applying the stress to utilize lead-lined gloves to limit radiation exposure. A weight-bearing ankle radiograph is also a stress view, as it applies a physiologic load to the joint. Recent studies have shown that weight-bearing films alone are adequate for determining the stability of ankle fractures, and that positive gravity stress radiographs may result in unnecessary surgical intervention [11, 17]. It is the authors' practice to only use gravity and manual stress radiographs when the patient is unable to receive a weight-bearing film, either due to pain or other disability, or when the weight-bearing radiographs are inconclusive (Fig. 6). From a practical perspective, these stress views can be obtained in the office, urgent care, or emergency department. When assessing ankle stability in the operating room, often the manual external rotation stress test is performed under fluoroscopic imaging, given the limits of patient positioning and participation.

Fig. 6 Due to polytrauma, this patient was unable to stand for a weight-bearing film. A manual external rotation stress demonstrated significant widening of the medial clear space via rotation and lateral translation of the unstable talus

Additional stress views also exist and are helpful for evaluating the ankle ligaments. The *anterior drawer stress* radiograph primarily evaluates the competency of the anterior talofibular ligament (ATFL) [7]. The ATFL is an important restraint to anterior subluxation of the talus, relative to the tibial plafond and is best evaluated using a lateral ankle radiograph. This can be obtained using specialized mechanical devices for applying the anterior drawer force, in a reproducible manner with a standardized force typically 15 kPa, or can be performed manually. When performed manually, the patient is positioned supine with the heel elevated on a firm bolster. Utilizing one hand to stabilize the tibia with a downward force, the second hand is placed behind the heel and pulls the foot forward [8]. A positive test will demonstrate anterior subluxation of the talus, with either 10 mm of absolute subluxation, or 3–5 mm of relative subluxation, compared to the contralateral side [20, 21]. The *talar tilt test*, or varus stress, primarily evaluates the integrity of the calcaneofibular ligament (CFL) by assessing the ankle's ability to resist a varus directed force. This is performed using an AP radiograph. While the patient is in the supine position, a varus force is manually applied through the ankle. The relative coronal plane angulation of the talus and the tibial plafond (talar tilt) is measured. Laxity of the lateral ankle ligaments will lead to greater talar tilt. The stress test is positive if there is 10° of talar tilt, or 3–5° of tilt relative to the contralateral ankle [20, 21]. The anterior drawer and talar tilt stress radiographs are certainly not a mandatory study for evaluating lateral ankle instability, as the diagnosis can be made based on history and physical examination. Studies have shown that these two stress views may underestimate the true severity of instability [20]. The images can, however, provide additional objective information to support the diagnosis and decision for treatment. Similarly, an ankle *valgus stress test* can be performed in an identical manner, providing information about the integrity of the deltoid ligament. This can be valuable in the setting of medial ankle instability or flatfoot reconstruction [22].

1.3 Specialized Radiographic Evaluations

Additional views, beyond the routine ankle series, can be helpful, and in some cases imperative for an adequate clinical assessment. Suggestion of injuries to the foot should certainly receive standard foot radiographs (AP, lateral, and external oblique). If one suspects a fracture to the calcaneus, two additional radiographs can be obtained to assess the fracture. The first is a *Harris (axial) heel* view, allowing one to visualize a longitudinal axial view of the calcaneus and the second is a *Broden* view, which provides further information about the subtalar joint integrity [8].

Suspected fractures of the talar neck can be evaluated with a *Canale view* radiograph. The *Canale* view is obtained by maximally plantarflexing the ankle and pronating the foot 15°. This allows for less obstructed visualization of the talar neck by reducing the overlap of the calcaneus on the talus. The *Canale* view is also useful for preoperative planning as well as postoperative assessment of reduction [23, 24].

Understanding the relationship between the hindfoot, ankle, and tibia is critical when planning for a deformity correction. A specialized radiograph that is helpful evaluating the ankle/hindfoot alignment and the presence of any coronal plane deformity is the *Saltzman hindfoot alignment view* (Fig. 7). Although visualization of the tibiotalar alignment is clear on the standard AP and lateral ankle radiographs, it does not provide a full assessment of the axial heel position

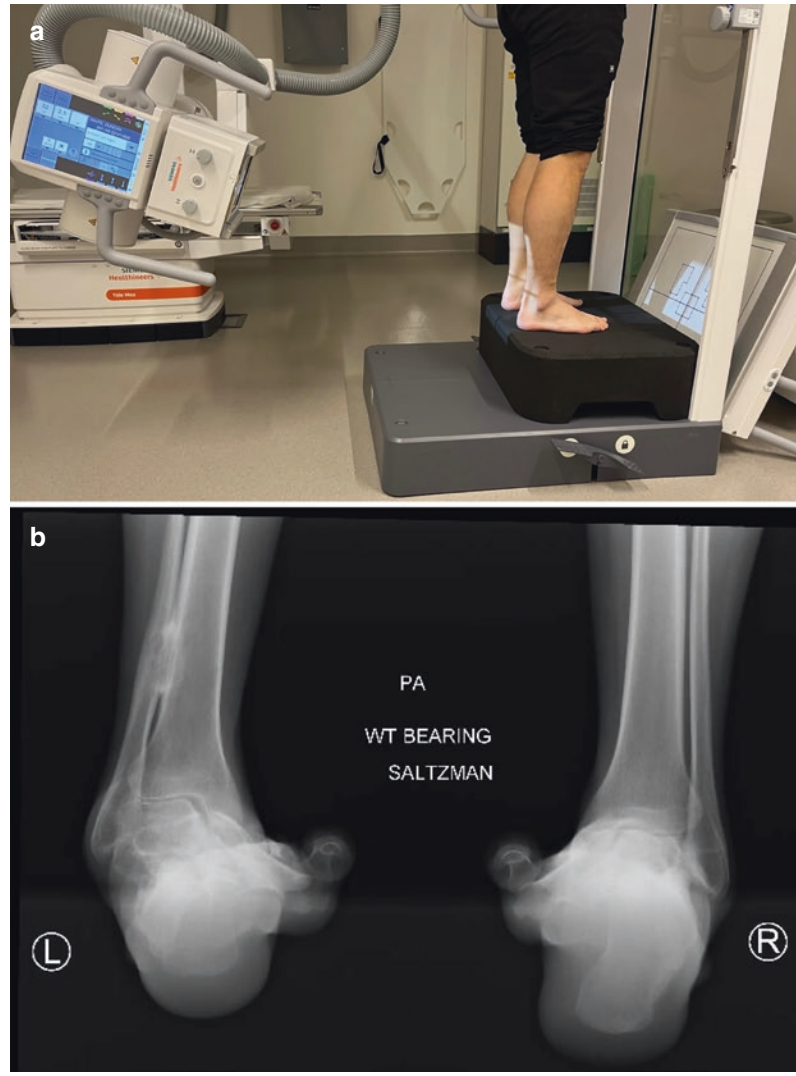

Fig. 7 Saltzman hindfoot alignment view: (**a**) The patient stands on a radiolucent platform. The cassette is angled 20° off the vertical, with the beam perpendicular to the cassette. (**b**) The Saltzman hindfoot alignment view shows significant hindfoot varus deformity in this patient

relative to the ankle and distal tibia. Multi-level deformity is not uncommon, and the Saltzman hindfoot alignment view provides a method for radiographically imaging the coronal plane alignment of the hindfoot in relation to the weight-bearing line of the tibia. With the patient standing, the beam is oriented in a posteroanterior direction and slightly plantar, 20° from the horizontal, with a detector cassette oriented 20° from the vertical [25, 26].

Lastly, *full-length extremity films*, also known as hip-to-calcaneus radiographs, are useful for evaluation of multilevel deformity as well as limb length discrepancies (Fig. 8) [27, 28]. They simultaneously provide information about coronal plane deformity at the femur, knee, tibia, ankle, and hindfoot. To obtain this radiograph, the patient stands on a radiolucent box while facing away from the beam with the patella centered. The beam is angled level to the horizontal at the level of the knee. The radiograph should project an image from the lower part of the pelvis through the calcaneus [27]. Mechanical and anatomic axis measurements can then be made to determine the necessary level(s) of correction. If both limbs are captured, leg length discrepancies can be measured. It has been shown surgical management of a deformity at the knee can have a direct impact on the improvement or exacerbation of deformity at the hindfoot and ankle [29].

Fig. 8 Full length alignment radiographs. Full length films are useful for assessing multiple levels of deformity, as well as for measuring leg length discrepancies

2 Magnetic Resonance Imaging

Magnetic resonance imaging (MRI) is an advanced imaging modality that is commonly used in the diagnosis of pathology around the foot and ankle. MRI technology uses magnetic fields and radio waves to collect data on a range of tissue characteristics, which is subsequently processed to produce a variety of different cross-sectional images [30]. MRI takes advantage of the magnetic properties of unpaired hydrogen protons in the targeted tissues. The magnet of the MRI produces a strong electromagnetic (EM) field, which causes the unpaired hydrogen atoms to align in a particular orientation [31]. Subsequently, a radiofrequency (RF) pulse is directed at the tissue, which causes the protons to enter a higher energy state. When the RF pulse ceases, the protons undergo relaxation, returning to their original energy state. In the process, they emit that energy differential in the form of RF energy, which maintains information about its source tissue. The MRI system detects the emitted RF energy and subsequently processes the data to produce images reflecting the unique biochemical tissue properties. The protons of muscle, fat, tendon, ligaments, bone, cartilage, and synovial fluid respond in different, but consistent ways to the MRI scanning process. This leads to

images with good differentiation between the various tissues, and potential for excellent definition of anatomic structures.

The way the MRI machine pulses RF energy affects the response of the unpaired protons in the imaged tissue. By controlling the variables around the pulsed RF energy, different MRI "sequences" can be obtained. Each sequence has unique characteristics that highlight different types of tissue (Fig. 9). Common examples include T1, T2, short tau inversion recovery (STIR), and proton density-weighted fast spin-echo (PD FSE) sequences [32]. The T1-weighted sequences display fat, subacute hemorrhage, and proteinaceous fluid as high signal, or bright, whereas edema and other fluid appears low signal, or dark [30]. A T1 image provides high anatomic detail and is useful for assessing findings like fracture lines, but is poor for evaluating cartilage. T2-weighted sequences display fluid as high signal and fat as low signal. They are important for looking for sites of edema. The PD-weighted FSE sequences provide high anatomic detail and, unlike T1 sequences, provide

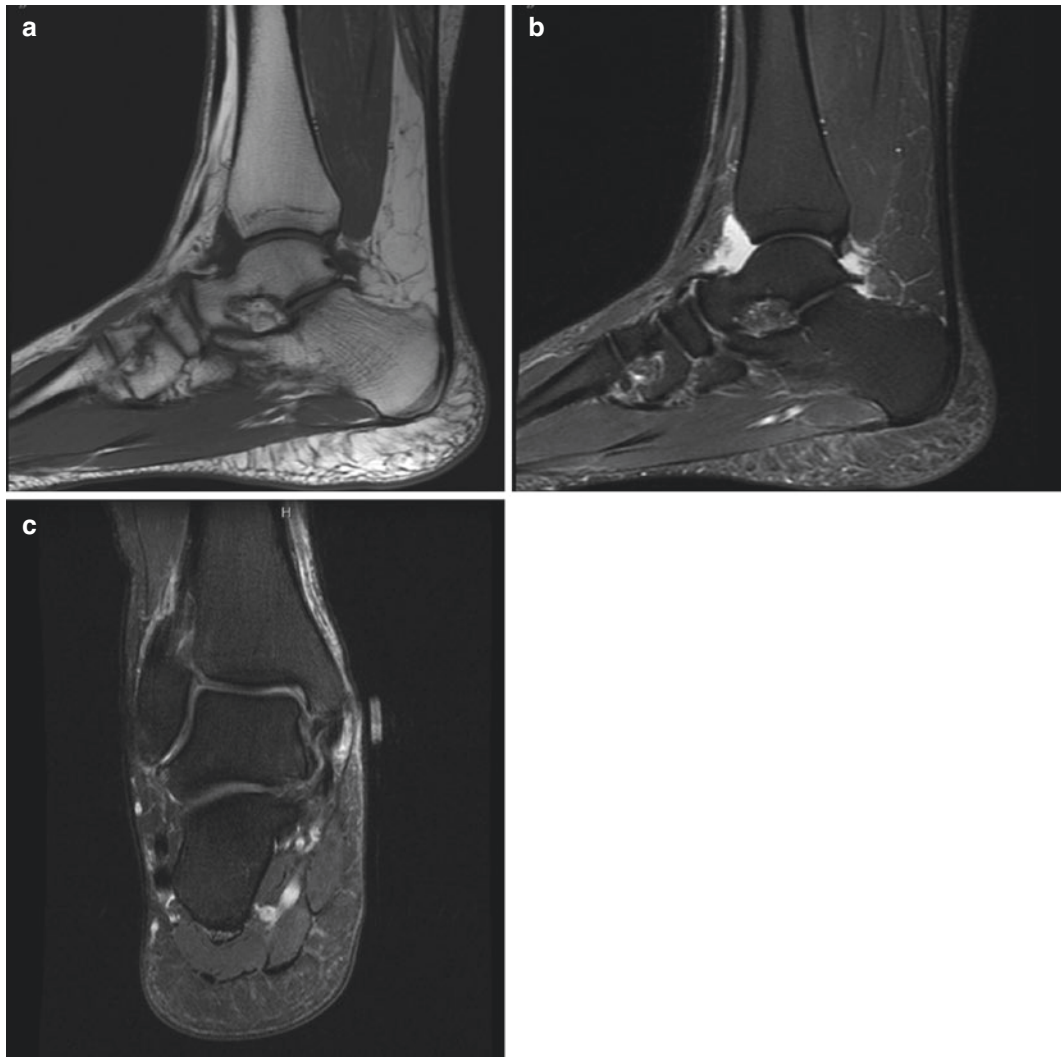

Fig. 9 Different MRI sequences highlight unique elements of patient anatomy and pathology. (**a**) T1 MRI image sagittal view of the ankle. (**b**) STIR MRI image sagittal view of the ankle. (**c**) PD MRI image coronal view of the ankle

excellent evaluation of articular cartilage. The STIR sequences highlight fluid, while suppressing fat, which is excellent for identifying edematous sites of pathology. Their long sequencing times, however, lead to worse resolution.

MRI is an important tool used in the evaluation of acute and chronic soft tissue, chondral, and osseous injuries. Often, given the close proximity of anatomic structures in the ankle and hindfoot, it can be difficult to definitively diagnose the exact source of a patient's symptoms on examination alone. For example, following inversion injuries (ankle sprains), an MRI can be useful for evaluating multiple adjacent structures simultaneously. MRI can assess the lateral ankle ligaments, the ATFL and CFL, as well as the syndesmosis for disruption. The peroneal tendons can be evaluated for tears, degeneration, or dislocation. Looking deeper, the tibiotalar joint may display osteochondral lesions of the talus and tibia, or synovitis with an associated ankle joint effusion. The adjacent hindfoot joints can also be assessed for chondral injury and potential coalitions. Similarly, medial sided pain can be assessed simultaneously for pathology of the deltoid ligament, posterior tibial tendon, tarsal tunnel, osteochondral lesions, medial malleolar stress fractures, among other possibilities. Thus, MRI can provide critical information to guide treatment.

In addition, MRI can aid in the diagnosis of an array of bony pathologies that may go unnoticed on plain radiographs. This includes bone marrow edema syndrome, stress fractures, as well as avascular necrosis (AVN) of the talus [33]. Furthermore, MRI, alongside radiographs and CT, is used to stage the progression of AVN, which can help guide future treatment [34].

Of particular interest, when considering MRI of the ankle, is the imaging of osteochondral lesions of the talus (OLT). Most OLTs occur in the talar dome, specifically in the posteromedial and centromedial aspect [35, 36]. Due its radiographic properties, MRI can reveal elements of bone edema, cyst formation, subchondral bone compression, cartilage delamination, and unstable osteochrondral fragments. Knowledge of the lesion's exact location, size, and depth, among other characteristics, is critical for determining operative positioning, approach, and treatment (Fig. 10) [37].

In addition, tendons are well visualized on MRI. Following lacerations or ruptures, the degree of tendon disruption and potential level of retraction can be determined. Evaluation for chronic pain can demonstrate various degrees of tendinopathy, in the form of peritendinous fluid, tendon thickening, split tears, and rupture. Although Achilles ruptures may be diagnosed by

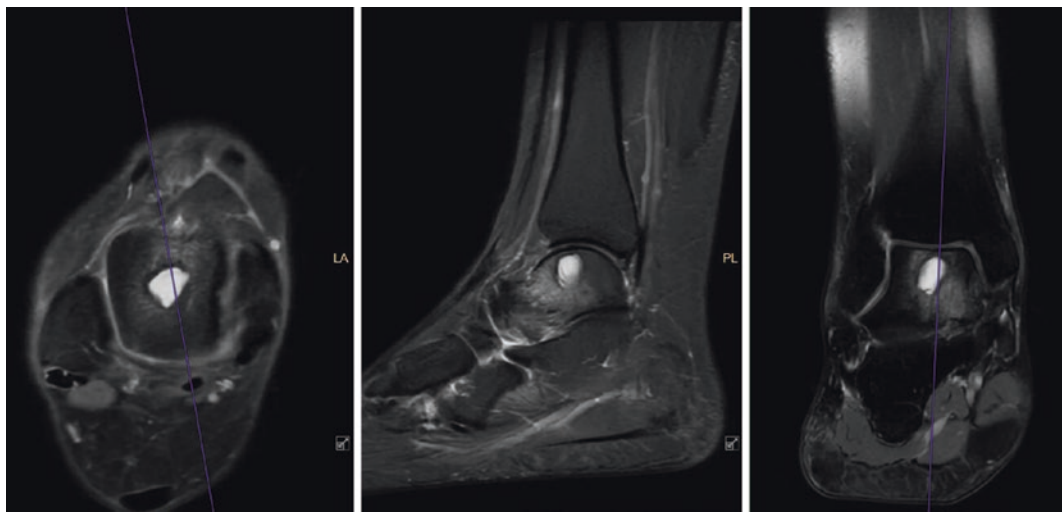

Fig. 10 MRI demonstrates a large talar subchondral cyst. Defining the location and size of the cyst is important for surgical planning

examination alone, an MRI with the ankle in plantarflexion can reveal the exact location of the rupture as well as evidence of tendon gapping, which may be important information when deciding on operative versus nonoperative management (Fig. 11) [38].

MRI is also an effective diagnostic modality for evaluating infection, as well as working up soft tissue and osseous masses. Though physical exam is a critical component of diagnosis, MRI can help define the extent and location of an infectious process. It can differentiate simple cellulitis from an abscess, or complex phlegmon. More importantly, MRI can provide evidence for underlying osteomyelitis, particularly when early or indolent, helping to guide operative management and antibiotic duration. When assessing masses about the foot and ankle, an MRI can define the structure, extent, and likely composition of soft tissue masses, to determine if the lesion is benign or malignant, and the need for excision versus staged biopsy versus observation. It can also provide further details about osseous lesions and reveal associated soft tissue components. When combined with an intravenous contrast, it is ideal for comprehensive assessment of tumors as well as lesion surveillance [39].

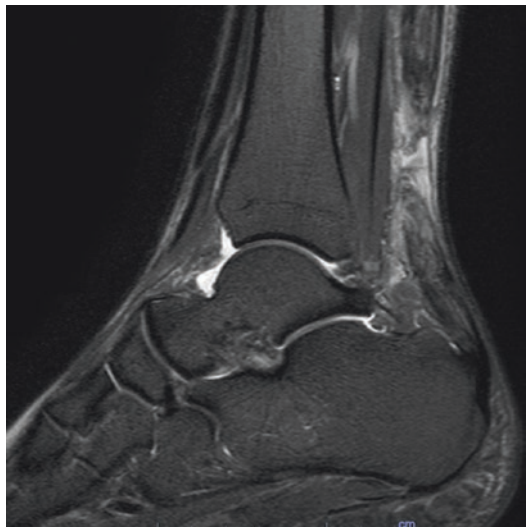

Fig. 11 MRI of the ankle demonstrates an acute Achilles rupture at its midsubstance. Gapping is noted between the tendon edges

3 Computed Tomography

Modern computed tomography (CT) allows for rapid acquisition of cross-sectional imaging. It can produce high resolution, thin-slice digital renderings of three-dimensional anatomic structures. At their core, CT scanners are composed of a gantry and a movable table [40]. The gantry is the frame that houses a rotating X-ray tube including collimators/filters, detectors, rotational components, angulation motors, and positioning laser lights. As the patient slides through the gantry aperture on the moving table, the rotating X-ray tube and detectors acquire image slices of the targeted anatomy. Modern helical or spiral CT scanner designs have multiple detectors, allowing the machine to acquire multiple slices with every rotation, effectively speeding up the required imaging time [41]. This process is termed "data acquisition." Three-dimensional CT images are broken up into small units of volume, or voxels. The amount of radiation that is absorbed, or attenuated, by each voxel of tissue dictates how it is displayed in the ultimate image rendering [30, 41]. The attenuation is then given a number based on a comparison with a similar voxel of water. For example, a voxel of bone will have higher attenuation than a voxel of gas in soft tissue. Each voxel in a CT slice is represented visually by a pixel on the two-dimensional slice renderings. The voxels are assigned values, known as Hounsfield units, based on their degree of X-ray attenuation. Hounsfield unit values represent the voxel's relative position on a visual gray scale [30]. At the extremes of the relative scale, dense bone will typically be white, while air will be black [41]. Through this process, the CT scanner can produce images with high resolution between different types of tissue. Due to the three-dimensional nature of the data acquisition, two-dimensional images can be reconstructed in multiple planes. Conventionally this is in the coronal, sagittal, and axial planes; however, the CT technologist can reformat slices in nearly any anatomic plane desired. The thinner the slices obtained, the higher the resolution in the various planes. The addition of picture archiving commu-

nication systems (PACS) has allowed higher-resolution scans to be obtained and stored.

A common concern with CT imaging is the inherent radiation exposure. Traditionally, a CT of the ankle delivered nearly fourfold the radiation of a chest radiograph [30]. Improvement in CT image resolution requires an increase in the density of voxels and number of slices. This, in turn, requires increased radiation exposure [41]. Fortunately, progress is being made to reduce radiation risks. Recent studies regarding radiation reduction protocols for the purpose of extremity trauma imaging have demonstrated tenfold reductions in exposure, relative to conventional protocols, without a significant sacrifice in resolution [42]. One study showed that their ankle fracture CT protocol exposed the subjects to less radiation than multiple views with conventional radiograph [43].

CT scans, which provide fine bony detail in multiple planes, and have become the standard of care for assessing a wide breadth of ankle pathology, from traumatic injury to tumors. Unlike a plain radiograph, which requires a fair amount of interpretation given the inherent bony overlap in the image, a CT can give definitive information about the three-dimensional status of the anatomy.

3.1 Fracture Management

CT imaging has proven to be highly advantageous in the evaluation of fractures about the ankle [44]. Injury patterns that often benefit from CT scanning include pilon fractures, malleolar ankle fractures, pediatric triplane and tillaux fractures, and talus fractures (Fig. 12) [30]. Providers can evaluate the size, location, and orientation of fragments involved, as well as the status of the joint surface, intra-articular fragments, and presence of bone loss. Another advantage of CT is the visualization of occult fractures that are otherwise not visible or very difficult to visualize on plain radiographs. They can also reveal soft tissue injuries, such as peroneal dislocation or soft tissue entrapment, helping with preoperative planning and having an important impact on surgical decision making. Studies have found that surgeons altered their surgical plans, including patient positioning and operative approach, in 23–44% of cases after obtaining CT imaging for rotational ankle fractures [45, 46]. The primary driving force for altering the surgical plan was the additional information obtained about the posterior malleolus fracture (Fig. 13). The additional use of three-dimensional reconstructions provides an intuitive rendering of the injury, akin to a physical model. Additionally, CTs can evaluate the quality of reduction either postoperatively or intraoperatively. One of the more common applications is to assess syndesmotic reduction in ankle fractures. Malreduction of the syndesmosis may be indicated for a revision of the previous fixation (Fig. 14) [47].

3.2 Supplementary Management

Osteochondral lesions of the talus (OLT) can be evaluated with CT as well as MRI. Although MRI is an important tool for detection of OLTs, it can often overestimate the size of the lesion, as bony edema is prominently displayed. CT is more precise in defining the bony involvement of the OLT, its size, cystic quality, and for guiding potential fixation in the acute setting [37]. CT arthrography is an alternative to MRI for evaluation of the chondral surface in the setting of patients with contraindications to MRI, such as an incompatible implanted cardiac device [30].

Evaluating bony union in the setting of fracture and fusion may be difficult due to obscuring hardware or overlapping bony projections, especially in cases like ankle fusions, subtalar fusions, or comminuted pilon fractures (Fig. 15). A CT can reveal all aspects of the joint, the fracture, or the fusion site, and can help visualize the degree of healing (with the exception of metal artifact).

Using intravenous (IV) contrast is an important adjunctive element of CT scans in select scenarios. In the acute setting, CT with contrast can confirm the level of a potential vascular disruption. It can also provide additional information about the blood flow to musculoskeletal tumors.

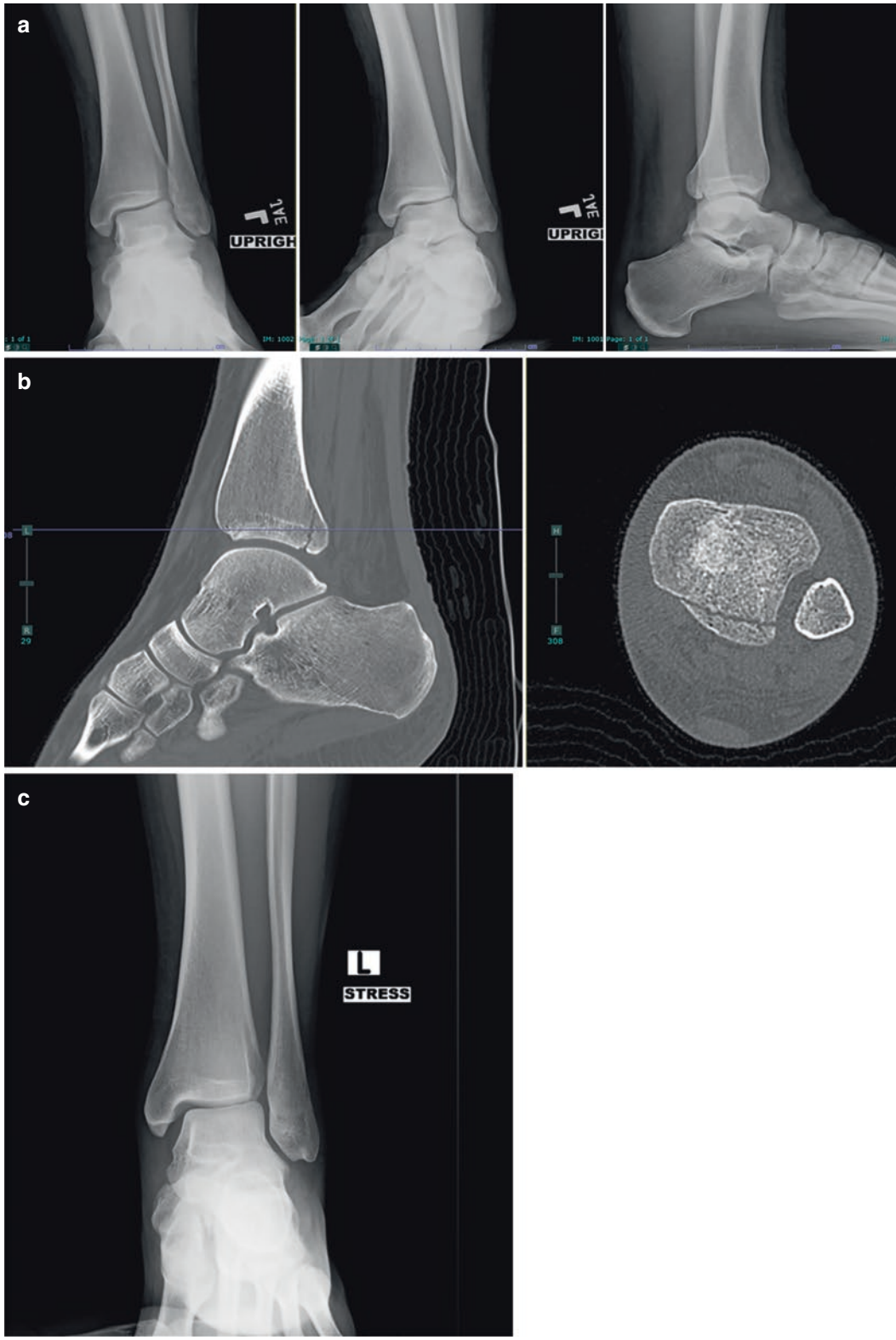

Fig. 12 CT scans are useful in assessing the size and morphology of malleolar fractures. (**a**) Radiographs demonstrate an isolated posterior malleolar fracture. (**b**) CT scan defines the size and orientation of the posterior malleolus fracture line. (**c**) Stress radiograph reveals medial clear space widening, suggestive of deltoid and syndesmotic instability

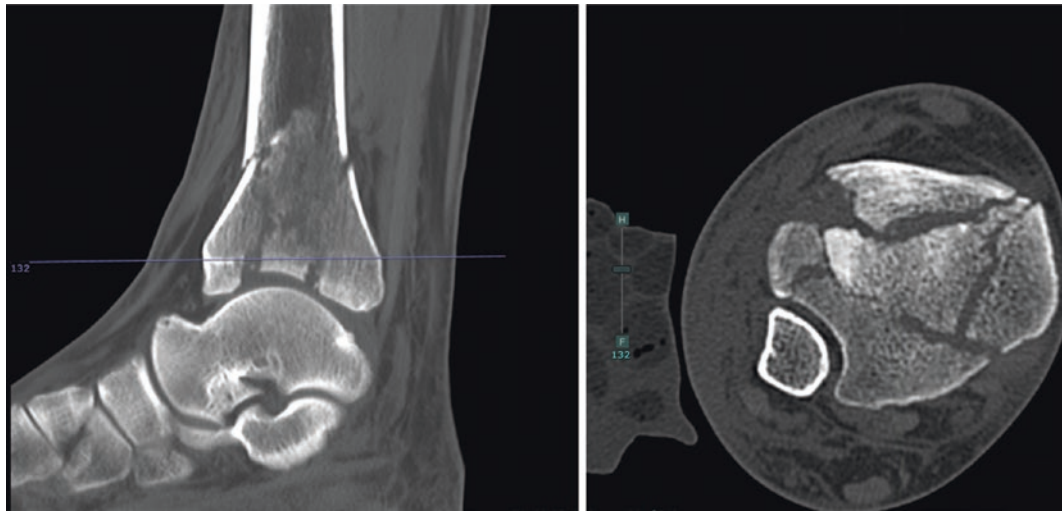

Fig. 13 CT of the ankle demonstrating a comminuted pilon fracture. Evaluation of the fracture in multiple planes is important for understanding the three-dimensional nature of the injury, particularly the location of fracture planes, independent fragments, and bone loss

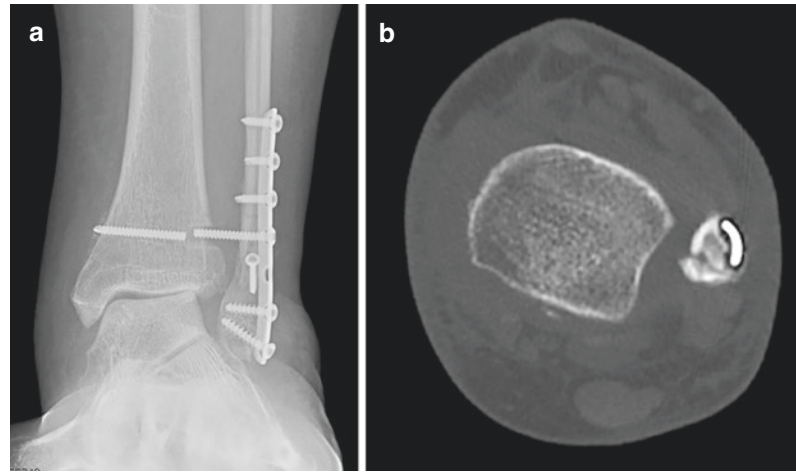

Fig. 14 CT imaging can demonstrate the presence of syndesmotic malreduction. (**a**) Mortise view radiograph suggesting syndesmotic disruption with failed hardware. (**b**) CT scan axial view demonstrates anterior translation of the fibula, with a malreduced syndesmosis

CT is an important adjunct in the diagnosis of ankle and hindfoot arthritis. It can reveal the extent of bone loss and the presence of bony cysts, which can affect surgical decision making, particularly when considering the use of a total ankle arthroplasty (TAA) [48]. Identifying significant bone loss in the talus, or the existence of large osteophytes can be used preoperatively as part of the surgical plan, while postoperatively it may detect peri-implant cysts (Fig. 16), component subsidence, loosening, a polyethylene fracture, or a malleolar fracture [49].

The advent of *weight bearing CT* (WBCT) technology has produced a paradigm shift in the evaluation of foot and ankle deformity. It effectively merges the valuable three-dimensional data of CT with the practical elements of a standing radiograph. One can view the bony anatomy, while also assessing the structural alignment of the foot and ankle under physiologic loading

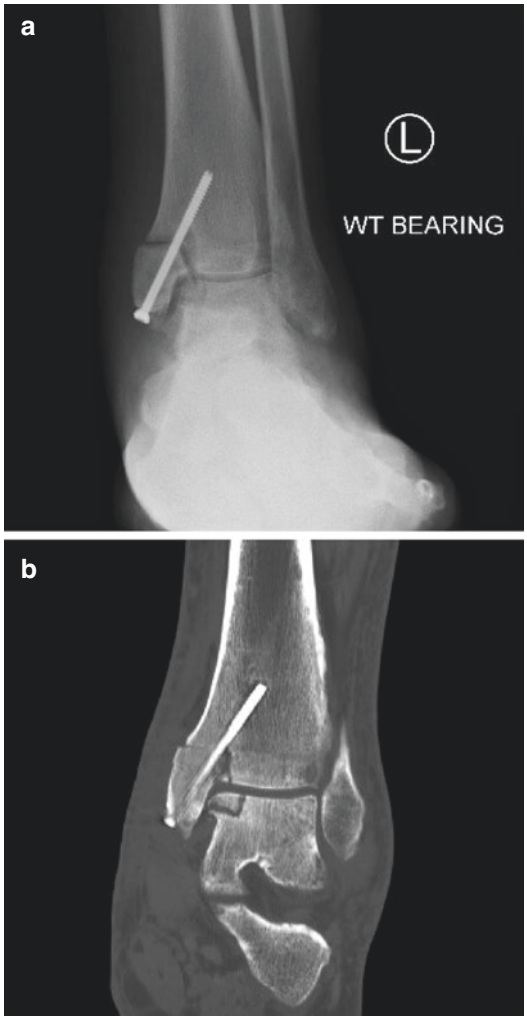

Fig. 15 Radiographs (**a**) demonstrate a nonunion of a prior medial malleolar osteotomy. A lucency is visible at the site of the medial talar osteochondral allograft, but it is unclear if it has united. (**b**) CT scan confirms nonunion of both the medial malleolus and the talar allograft

(Fig. 17). This has been particularly beneficial in evaluating the subtalar joint and subfibular impingement. This improves the physician's understanding of the relative position of the

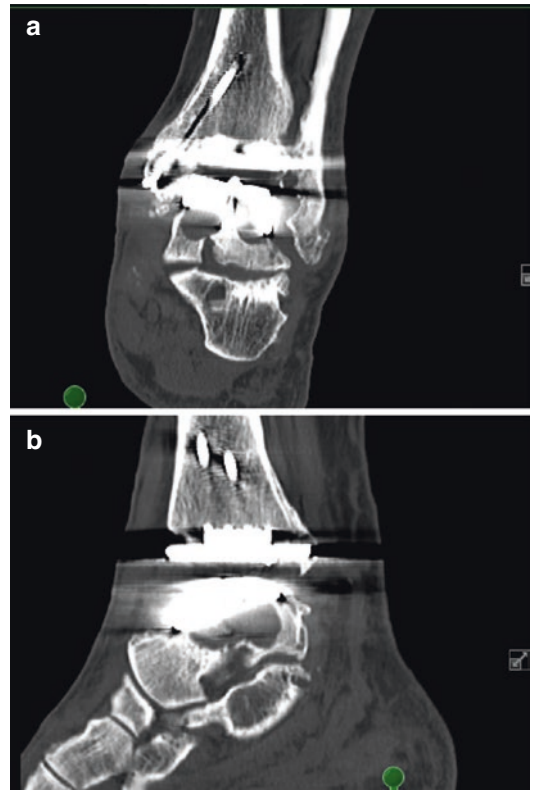

Fig. 16 CT demonstrating large talar cysts adjacent to the talar component of a total ankle replacement. (**a**) Coronal view. (**b**) Sagittal view

bones and joints in their weight-bearing state when patients experience pain or dysfunction. It is valuable for evaluating post-traumatic malunion, ankle and hindfoot arthritis with associated malalignment, as well as complex and potentially dynamic deformities such as progressive collapsing foot deformity, and conditions like Charcot Marie Tooth disease [50, 51]. This effectively raises the bar with regards to clinical diagnosis and preoperative planning and provides insights that would not be available using non-weight-bearing CT scans.

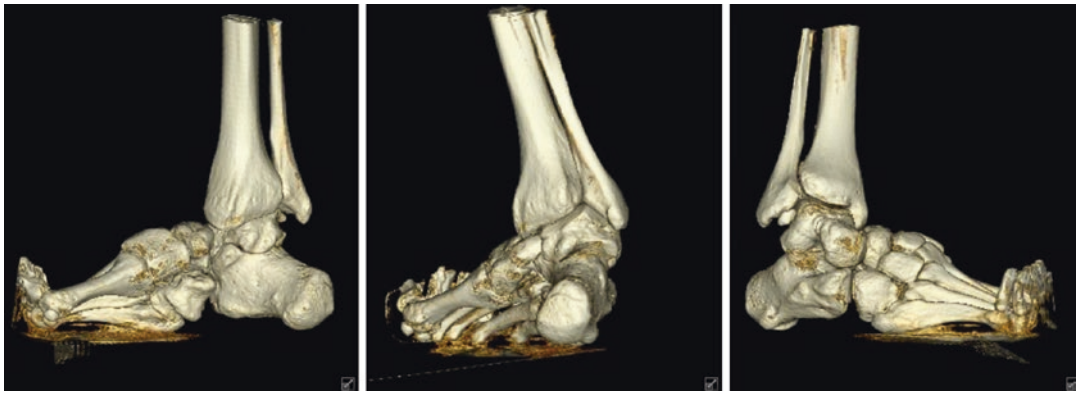

Fig. 17 Weight-bearing CT imaging allows for visualization of foot and ankle alignment under physiologic loading. This is valuable for understanding deformity and planning surgical correction. Furthermore, 3-dimensional reconstruction views give the provider a practical rendering of the patient's anatomy

4 Ultrasound

Ultrasound allows for real-time, dynamic imaging of the foot and ankle. It works in a manner similar to naval SONAR (sound navigation and ranging) systems, in which sound waves are emitted, reflected, and subsequently detected, providing information about the structures they encounter [30]. Ultrasound transducers produces high-frequency sound waves in the range of 5–18 MHz. As air can cause disturbances in image acquisition, ultrasound gel is placed between the probe and the patient's skin. Alternatively, the anatomy of interest can be submersed in liquid. Ultrasonic waves are passed from the probe into the tissue, reflecting at different acoustic interfaces. With these reflected echoes, the ultrasound system can produce a diagnostic image in real-time. In general, higher frequency probes produce high detail, but limited depth of imaging. Low frequency probes produce lower resolution but can detect structures at greater depths.

Ultrasound use has good musculoskeletal applications including the evaluations of tendons, nerves, and allowing guidance to ensure accurate targeted injections. When used for the evaluation of tendons, it can diagnose, in real-time, the pathology of the tendons. The peroneal tendons can be evaluated for split tears and tenosynovitis, with the patient actively moving, along with subluxation and dislocation. The Achilles tendon can also be reliably imaged, with some studies showing 96% accuracy for diagnosing a full rupture [38, 52]. Combining physical examination with real-time ultrasound improves diagnostic accuracy [53].

It can also evaluate a variety of nerve pathologies about the ankle and hindfoot by allowing direct visualization of the course of the nerve. Often, if there is a nerve entrapment, structural changes can be seen at typical compression sites, such as passing through fascial planes. Entrapment will create a typical appearance of swelling proximal to the compression site, with return of normal caliber distal to the site [52]. This is specifically helpful for the evaluation of tarsal tunnel syndrome. Not only can direct nerve changes be detected, but ultrasound can also show compressive lesions, like ganglions or enlarged vessels, as well as scar tissue formation.

In addition to identifying the musculoskeletal pathologies, many providers utilize ultrasound guidance when performing targeted injections to ensure accuracy, whether into the tibiotalar joint or around tendons. Similarly, cystic masses, like ganglions, can be visualized so that an accurate aspiration is performed [52]. Another use for ultrasound is assessing for and localizing the presence of a foreign body, especially those that are radiolucent, such as a splinter.

Lastly, although not an ankle injury, ultrasound is the most common modality used to confirm a deep venous thrombosis (DVT) of the leg [54].

5 Nuclear Medicine

Nuclear Medicine is a unique imaging modality that is utilized to diagnose pathology that would be otherwise undetectable on conventional radiographs, like stress fractures and osteomyelitis [30]. It has also gained value in the workup of painful total ankle replacements, to help localize the offending source of pain. Nuclear scans require the injection of radioactive agents into the patient prior to imaging. There are various radiopharmaceutical agents available for an array of diagnostic purposes. They are labeled with ligands, which are ions, molecules, or functional groups that bind to another chemical entity to form a larger complex, during specific physiologic processes. Once injected, the nuclear agents generally have preferential uptake in sites of elevated metabolic activity, leading to a localized concentration [55]. By their nature, the agents emit radioactive energy. A gamma camera detects the emission, and after converting the radioactive energy to photos, ultimately produces a visual representation of the localized radiopharmaceutical uptake in the body. Although relatively crude in appearance, these images are unique in their ability to represent a physiologic process.

Technetium-99m-methylene diphosphate *bone scans* are useful for detecting sites of increased osteoblastic activity, such as fractures, tumors, and growth plates. As such it can be utilized to detect stress fractures, bony tumors, and osteochondral injuries [30, 56]. Indium-111, as well as technetium-99m, can be utilized for white blood cell-tagged studies for evaluation of osteomyelitis (Fig. 18) [30]. When investigating for an infection, the radiopharmaceutical agent is incubated

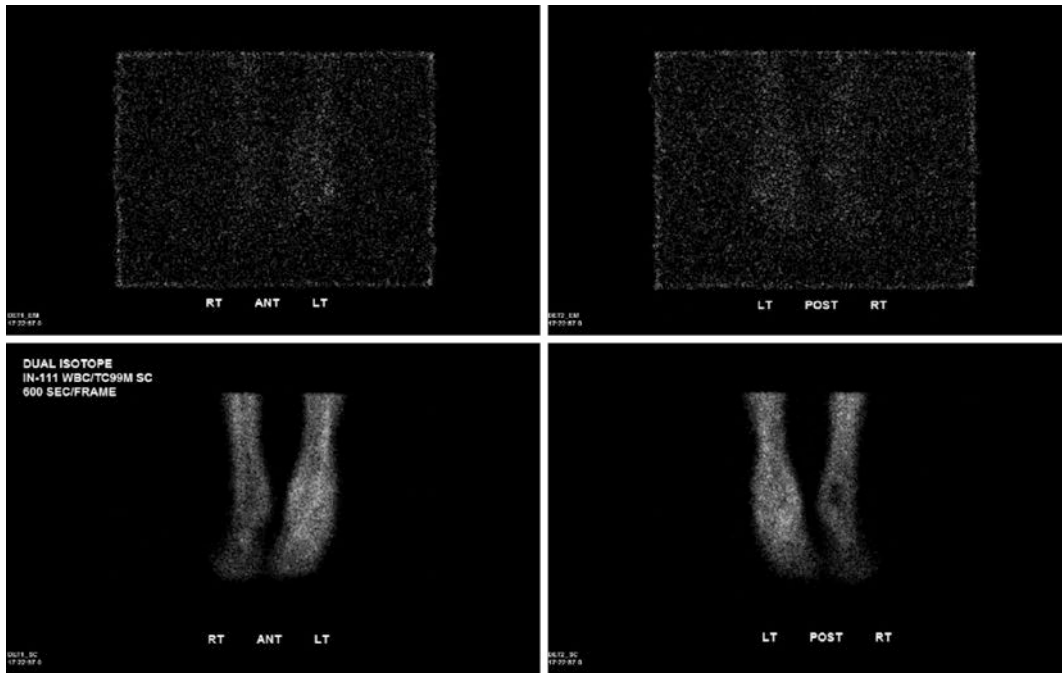

Fig. 18 Indium-111 white blood cell-tagged study performed to rule out osteomyelitis of the distal tibia. In this case, the lack of signal suggests no active infection

with isolated leukocytes with isolated leukocytes from the patient's blood draw. They are then reinjected, and the leukocytes will tend to concentrate in areas of active infection, such as an area of suspected osteomyelitis. The patient will undergo scanning at 4 and 24 h following the injection. The resultant images will demonstrate focal uptake in the event of infection. Charcot arthropathy can often be particularly difficult to differentiate from osteomyelitis with a high false positive rate with both MRI and routine bone scan. The advent of dual bone scans, utilizing Indium-111 labeled white blood cells alongside technetium-99 sulfur colloid has improved the specificity of nuclear scans for diagnosing osteomyelitis to differentiate from an acute Charcot arthropathy [57].

An increasingly valuable imaging modality is single photon emission computed tomography (SPECT). Unlike the crude images rendered in traditional bone scans, SPECT can blend the clarity of modern CT imaging with the functional data obtained from nuclear medicine. Its primary advantage is being able to pinpoint sites of increased metabolic activity. This is particularly helpful after patients have undergone complex surgery, where pain is diffuse, and there are many potential sources of pain. An important application is in the work up of painful total ankle arthroplasty [58, 59]. In these patients, their postoperative pain could be secondary to component subsidence, loosening, cyst formation (at multiple sites), impingement, stress fracture, and infection, among others (Fig. 19). SPECT can help the physician localize the most likely origin of symptoms.

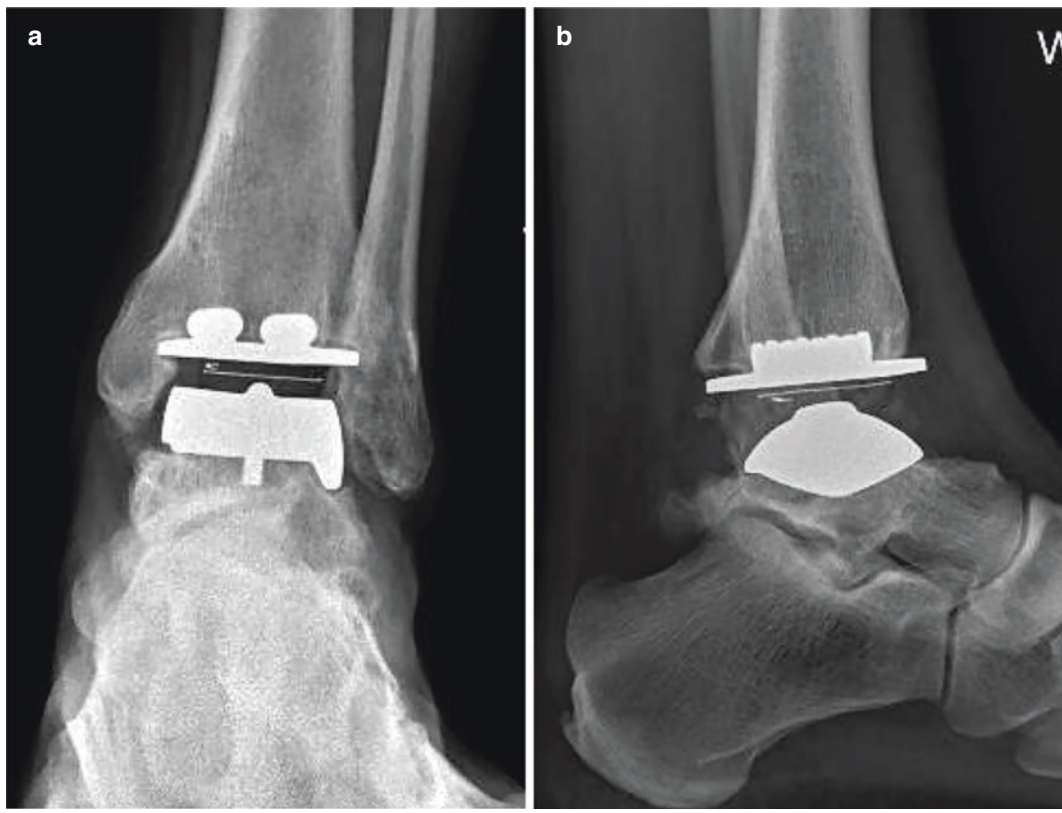

Fig. 19 SPECT imaging is valuable for diagnosing the source of pain in total ankle arthroplasty. (**a**, **b**) Radiographs suggest a potential lucency under the talar component but are inconclusive. (**c**, **d**) SPECT scan demonstrates increased signal under the talar component. The CT confirmed a large cyst

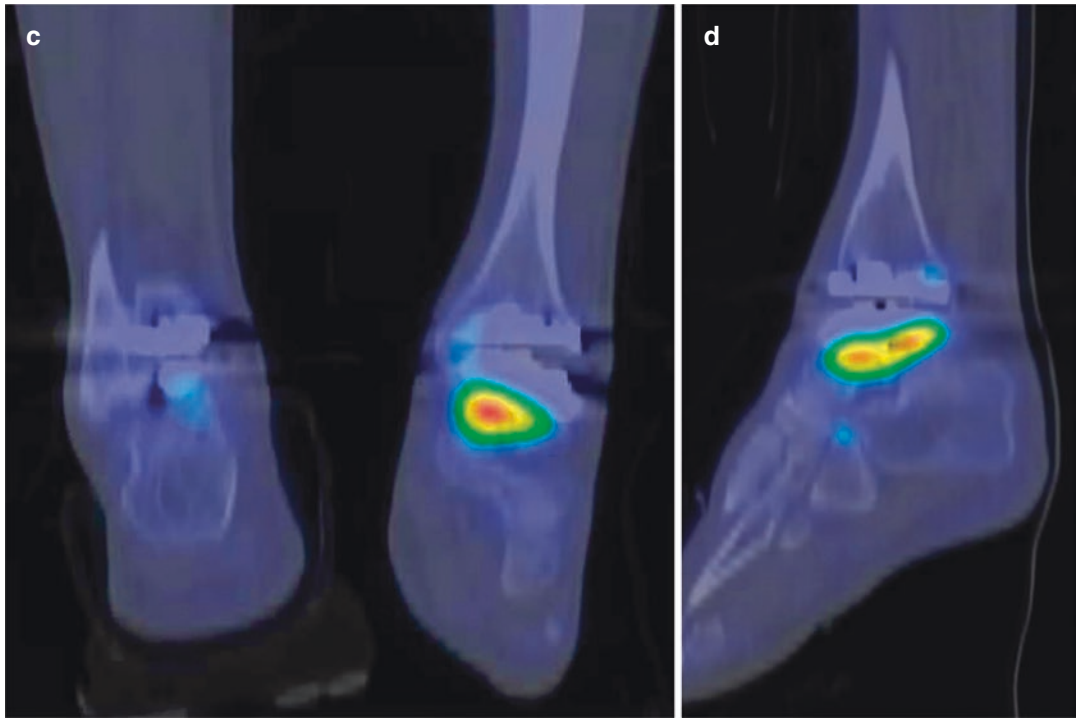

Fig. 19 (continued)

6 Conclusion

There are many options when it comes to imaging of the ankle. As such, the provider must be prudent with their diagnostic workups. Factors such as radiation exposure, patient burden, and cost should not be overlooked. As such, it is important to have clear indications for the various imaging modalities. When doing an initial evaluation of ankle pain or instability, it is the author's opinion that a routine weight-bearing ankle series is nearly always appropriate and can provide significant information about osseous injury and quality, joint degeneration, ligamentous stability, and overall alignment of the ankle and hindfoot. Synthesizing information from the patient's history, examination, and radiographs, the provider can then determine the need for further imaging. The judicious use of CT, MRI, nuclear scans, and ultrasound can provide unique data that can assist with diagnosis, treatment choice, and nuances of surgical planning.

References

1. Chotas HG, Dobbins JT III, Ravin CE. Principles of digital radiography with large-area, electronically readable detectors: a review of the basics. Radiology. 1999;210(3):595–9.
2. Bushberg JT. The essential physics of medical imaging. 3rd ed. Philadelphia, PA: Wolters Kluwer Health/Lippincott Williams & Wilkins; 2012.
3. Stiell IG, Greenberg GH, McKnight RD, Nair RC, McDowell I, Reardon M, et al. Decision rules for the use of radiography in acute ankle injuries. Refinement and prospective validation. JAMA. 1993;269(9):1127–32.
4. Bachmann LM, Kolb E, Koller MT, Steurer J, ter Riet G. Accuracy of Ottawa ankle rules to exclude fractures of the ankle and mid-foot: systematic review. BMJ. 2003;326(7386):417.
5. Morais B, Branquinho A, Barreira M, Correia J, Machado M, Marques N, et al. Validation of the Ottawa ankle rules: strategies for increasing specificity. Injury. 2021;52(4):1017–22.
6. Stiell IG, McKnight RD, Greenberg GH, McDowell I, Nair RC, Wells GA, et al. Implementation of the Ottawa ankle rules. JAMA. 1994;271(11):827–32.
7. Berquist TH. Imaging of the foot and ankle. 3rd ed. Philadelphia, PA: Wolters Kluwer/Lippincott Williams & Wilkins Health; 2011.

8. Degwert R, Gaulrapp H, Kessler S, Roeser A, Staebler A, Szeimies U, et al. Diagnostic imaging of the foot and ankle. Stuttgart: Thieme; 2015.
9. Lau BC, Allahabadi S, Palanca A, Oji DE. Understanding radiographic measurements used in foot and ankle surgery. J Am Acad Orthop Surg. 2022;30(2):e139–e54.
10. Ebraheim NA, Wong FY. External rotation views in the diagnosis of posterior colliculus fracture of the medial malleolus. Am J Orthop. 1996;25(5):380–2.
11. Gregersen MG, Molund M. Weightbearing radiographs reliably predict normal ankle congruence in weber B/SER2 and 4a fractures: a prospective case-control study. Foot Ankle Int. 2021;42(9):1097–105.
12. Murphy JM, Kadakia AR, Irwin TA. Variability in radiographic medial clear space measurement of the normal weight-bearing ankle. Foot Ankle Int. 2012;33(11):956–63.
13. Arthur D, Pyle C, Shymon SJ, Lee D, Harris T. Correlating arthroscopic and radiographic findings of deep deltoid ligament injuries in rotational ankle fractures. Foot Ankle Int. 2021;42(3):251–6.
14. Cavanaugh ZS, Gupta S, Sathe VM, Geaney LE. Initial fibular displacement as a predictor of medial clear space widening in weber B ankle fractures. Foot Ankle Int. 2018;39(2):166–71.
15. Shah AS, Kadakia AR, Tan GJ, Karadsheh MS, Wolter TD, Sabb B. Radiographic evaluation of the normal distal tibiofibular syndesmosis. Foot Ankle Int. 2012;33(10):870–6.
16. Harper MC, Keller TS. A radiographic evaluation of the tibiofibular syndesmosis. Foot Ankle. 1989;10(3):156–60.
17. Seidel A, Krause F, Weber M. Weightbearing vs gravity stress radiographs for stability evaluation of supination-external rotation fractures of the ankle. Foot Ankle Int. 2017;38(7):736–44.
18. McConnell T, Creevy W, Tornetta P. Stress examination of supination external rotation-type fibular fractures. J Bone Joint Surg Am. 2004;86(10):2171–8.
19. Park SS, Kubiak EN, Egol KA, Kummer F, Koval KJ. Stress radiographs after ankle fracture: the effect of ankle position and deltoid ligament status on medial clear space measurements. J Orthop Trauma. 2006;20(1):11–8.
20. Hoffman E, Paller D, Koruprolu S, Drakos M, Behrens SB, Crisco JJ, et al. Accuracy of plain radiographs versus 3D analysis of ankle stress test. Foot Ankle Int. 2011;32(10):994–9.
21. Jolman S, Robbins J, Lewis L, Wilkes M, Ryan P. Comparison of magnetic resonance imaging and stress radiographs in the evaluation of chronic lateral ankle instability. Foot Ankle Int. 2017;38(4):397–404.
22. Francisco R, Chiodo CP, Wilson MG. Management of the rigid adult acquired flatfoot deformity. Foot Ankle Clin. 2007;12(2):317–27, vii.
23. Thomas JL, Boyce BM. Radiographic analysis of the Canale view for displaced talar neck fractures. J Foot Ankle Surg. 2012;51(2):187–90.
24. Canale ST, Kelly FB. Fractures of the neck of the talus. Long-term evaluation of seventy-one cases. J Bone Joint Surg Am. 1978;60(2):143–56.
25. Saltzman CL, El-Khoury GY. The hindfoot alignment view. Foot Ankle Int. 1995;16(9):572–6.
26. Cobey J. Posterior roentgenogram of the foot. Clin Orthop Relat Res. 1976;118:202–7.
27. Haraguchi N. Analysis of whole limb alignment in ankle arthritis. Foot Ankle Clin. 2022;27(1):1–12.
28. Kim J, Rajan L, Kumar P, Kim JB, Lee WC. Lower limb alignment in patients with primary valgus ankle arthritis: a comparative analysis with patients with varus ankle arthritis and healthy controls. Foot Ankle Surg. 2022;29:72.
29. Mansur H, Rocha FA, Garcia PBL, de Alencar FHU, Guilme P, de Castro IM. Alteration of hindfoot axis after total knee arthroplasty. J Arthroplast. 2019;34(10):2376–82.
30. Coughlin M, Saltzman C, Anderson R. Mann's surgery of the foot and ankle, vol. 2. 9th ed. Amsterdam: Elsevier Health Sciences; 2014.
31. Anderson J, Read J. Atlas of imaging in sports medicine. Sydney, NSW: McGraw-Hill Education Australia; 2016.
32. Grover VP, Tognarelli JM, Crossey MM, Cox IJ, Taylor-Robinson SD, McPhail MJ. Magnetic resonance imaging: principles and techniques: lessons for clinicians. J Clin Exp Hepatol. 2015;5(3):246–55.
33. Orr JD, Sabesan V, Major N, Nunley J. Painful bone marrow edema syndrome of the foot and ankle. Foot Ankle Int. 2010;31(11):949–53.
34. Zhang H, Fletcher AN, Scott DJ, Nunley J. Avascular osteonecrosis of the talus: current treatment strategies. Foot Ankle Int. 2022;43(2):291–302.
35. Pedowitz R, Chung CB, Resnick D. Magnetic resonance imaging in orthopedic sports medicine. 1st ed. Berlin: Springer; 2008.
36. van Diepen PR, Dahmen J, Altink JN, Stufkens SAS, Kerkhoffs GMMJ. Location distribution of 2,087 osteochondral lesions of the talus. Cartilage. 2021;13(1 Suppl):1344S–53S.
37. Wodicka R, Ferkel E, Ferkel R. Osteochondral lesions of the ankle. Foot Ankle Int. 2016;37(9):1023–34.
38. Dams OC, Reininga IHF, Gielen JL, van den Akker-Scheek I, Zwerver J. Imaging modalities in the diagnosis and monitoring of Achilles tendon ruptures: a systematic review. Injury. 2017;48(11):2383–99.
39. Rammelt S, Fritzsche H, Hofbauer C, Schaser KD. Malignant tumours of the foot and ankle. Foot Ankle Surg. 2020;26(4):363–70.
40. Mazonakis M, Damilakis J. Computed tomography: what and how does it measure? Eur J Radiol. 2016;85(8):1499–504.
41. Seeram E. Computed tomography: a technical review. Radiol Technol. 2018;89(3):279CT–302CT.
42. Konda SR, Goch AM, Haglin J, Egol KA. Ultralow-dose CT (reduction protocol) for extremity fracture evaluation is as safe and effective as conventional CT: an evaluation of quality outcomes. J Orthop Trauma. 2018;32(5):216–22.

43. Tuncer K, Topal M, Tekin E, Sade R, Pirimoglu RB, Polat G. The new ultralow dose CT protocol for the diagnosis of fractures of the ankle: a prospective comparative study with conventional CT. J Orthop Surg. 2020;28(3):2309499020960238.
44. Rammelt S, Boszczyk A. Computed tomography in the diagnosis and treatment of ankle fractures: a critical analysis review. JBJS Rev. 2018;6(12):e7.
45. Donohoe S, Alluri RK, Hill JR, Fleming M, Tan E, Marecek G. Impact of computed tomography on operative planning for ankle fractures involving the posterior malleolus. Foot Ankle Int. 2017;38(12):1337–42.
46. Kumar A, Mishra P, Tandon A, Arora R, Chadha M. Effect of CT on management plan in malleolar ankle fractures. Foot Ankle Int. 2018;39(1):59–66.
47. Sagi HC, Shah AR, Sanders RW. The functional consequence of syndesmotic joint malreduction at a minimum 2-year follow-up. J Orthop Trauma. 2012;26(7):439–43.
48. Cody EA, Scott DJ, Easley ME. Total ankle arthroplasty: a critical analysis review. JBJS Rev. 2018;6(8):e8.
49. Lee GW, Lee KB. Periprosthetic osteolysis as a risk factor for revision after total ankle arthroplasty: a single-center experience of 250 consecutive cases. J Bone Joint Surg Am. 2022;104(15):1334–40.
50. Barg A, Bailey T, Richter M, de Cesar Netto C, Lintz F, Burssens A, et al. Weightbearing computed tomography of the foot and ankle: emerging technology topical review. Foot Ankle Int. 2018;39(3):376–86.
51. Michalski MP, An TW, Haupt ET, Yeshoua B, Salo J, Pfeffer G. Abnormal bone morphology in Charcot-Marie-tooth disease. Foot Ankle Int. 2022;43(4):576–81.
52. Beard NM, Gousse RP. Current ultrasound application in the foot and ankle. Orthop Clin North Am. 2018;49(1):109–21.
53. Griffin MJ, Olson K, Heckmann N, Charlton TP. Realtime Achilles ultrasound Thompson (RAUT) test for the evaluation and diagnosis of acute Achilles tendon ruptures. Foot Ankle Int. 2017;38(1):36–40.
54. Bright JM, Fields KB, Draper R. Ultrasound diagnosis of calf injuries. Sports Health. 2017;9(4):352–5.
55. Waller ML, Chowdhury FU. The basic science of nuclear medicine. Orthop Trauma. 2016;30(3):201–22.
56. Leumann A, Valderrabano V, Plaass C, Rasch H, Studler U, Hintermann B, et al. A novel imaging method for osteochondral lesions of the talus--comparison of SPECT-CT with MRI. Am J Sports Med. 2011;39(5):1095–101.
57. Womack J. Charcot arthropathy versus osteomyelitis: evaluation and management. Orthop Clin. 2017;48(2):241–7.
58. Mason LW, Wyatt J, Butcher C, Wieshmann H, Molloy AP. Single-photon-emission computed tomography in painful total ankle replacements. Foot Ankle Int. 2015;36(6):635–40.
59. Vulcano E, Myerson MS. The painful total ankle arthroplasty: a diagnostic and treatment algorithm. Bone Joint J. 2017;99B(1):5–11.